CHAPTER SEVEN

Modeling Turbulent Bore Propagation in the Surf Zone

David R. Basco[1] and Ib A. Svendsen[2]

Abstract

Initial efforts to numerically simulate surf zone waves by using
a modified form of the nonlinear shallow water equations are des-
cribed. Turbulence generated at the front of the moving bore-like
wave spreads vertically downward to significantly alter the velocity
profile and hence the horizontal momentum flux. This influence of
turbulence is incorporated into the momentum balance equation through
a momentum correction coefficient, α which is prescribed based in part
upon the theoretical $\alpha(x)$ distribution beneath stationary hydraulic
jumps. The numerical results show that with a suitably chosen $\alpha(x)$
distribution, the equations not only dissipate energy as the waves
propagate, but also that the wave shape stabilizes as a realistic pro-
file rather than progressively steepening as when the nonlinear shal-
low water equations are employed. Further research is needed to theo-
retically determine the appropriate $\alpha(x,t)$ distribution.

1. Introduction

The transformation of breaking and broken waves in the surf zone
is the dominant factor in the hydrodynamics of nearshore circulation,
runup and sediment transport. Development of rational theories to
describe breaking waves is just beginning.

After the moment the plunging jet strikes the onrushing trough,
the wave undergoes a rapid transition in the region termed the outer
surf zone (Fig. 1). Soon a bore-like shape appears which is main-
tained onto the beach or onto a bar profile as long as the depth de-
creases. This inner surf zone region involves the propagation of un-
steady bores of non-constant form as they shoal, dissipate energy and
create a mean water level setup on the beach.

This paper describes initial efforts to numerically model surf
zone waves by using a modified form of the nonlinear shallow water
equations (SWE) with additional momentum flux induced by the mean
velocity profile through the bore. Numerical integration is by the
fininte-difference method and emphasis is on the many factors in-
fluencing the numerical results when compared with laboratory data.

[1]Professor, Civil and Ocean Engineering, Texas A&M University, College
Station, TX 77843.
[2]Professor, Institute of Hydrodynamics and Hydraulic Engineering
(ISVA), Technical University of Denmark, Building 115, DK-2800,
Lyngby, Denmark.
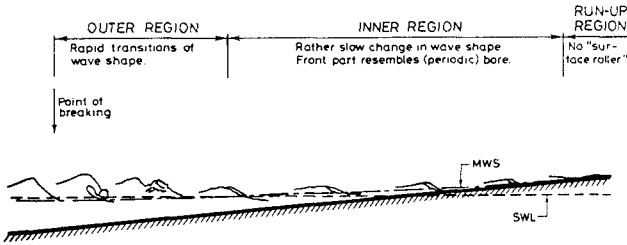
Fig. 1   Wave characteristics in the surf zone. (from Svendsen, et al., 1978)
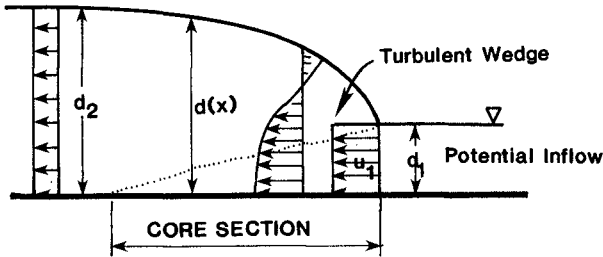
Fig. 2   Moving bores and jumps – relative coordinate system.
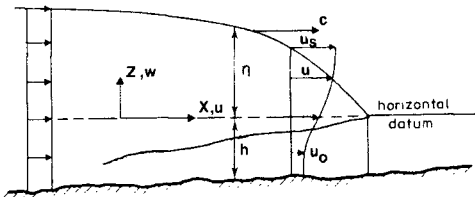
Fig. 3   Nonconstant form bores – fixed coordinate system.

An early approach to this problem idealized the moving bore front as a sharp discontinuity in the flow and used a "shock-fitting" procedure from classic hydraulic jump theory across the front (Meyer and Taylor, 1972, give a review). Others (Lax and Wendroff, 1960; Hibberd and Peregrine, 1979) rely on numerical viscosity induced by the coarse grid resolution at the front to produce a dissipative effect. Both methods do not permit details of the front wave shape nor internal dynamics to be resolved and consequently the wave propagation celerity is questionable.

As physically demonstrated by Peregrine and Svendsen (1978), turbulence is generated at the "toe" or front of the moving bore and spreads vertically to significantly influence the velocity profile in this high shear flow region. Madsen and Svendsen (1983) quantify this concept to develop an analytical model for steady flow, classic hydraulic jumps or moving bores on constant water depth. Turbulence closure is by a one-equation $(k-\varepsilon)$ theory for transport of turbulent kinetic energy. The mixing-length is related to the turbulent wedge (Fig. 2) spreading from the surface at the toe and adjusting the similarity velocity profile in the downstream direction. Four dependent variables result that require solution of the depth-integrated continuity, total momentum, energy, and potential core-region momentum (Bernoulli) equations.

These ideas and methods were generalized and extended to unsteady, non-permanent form, propagating bores by Svendsen and Madsen (1984, in review). In a fixed frame of reference, a hyperbolic system of four simultaneous partial differential equations result. Additional turbulence closure relations are also required. Specification of the boundary conditions becomes difficult for the numerical solution of the four equation system. Without turbulence, the four equations reduce to the SWE.

In the present paper we only consider the depth-integrated equations of continuity and total momentum and include the influence of turbulence on the momentum flux through a momentum correction coefficient, α which is prescribed. The purpose is to show that with a suitably chosen $\alpha(x)$ - distribution, the equations will not only dissipate energy as the waves propagate, but the wave shape will stabilize as a realistic profile instead of progressively steepening as when the ordinary SWE are employed.

The basic equations of the four equation system are summarized in Section 2, where the theory for the two equation method is also presented. Section 3 summarizes the theoretical $\alpha(x)$ - distribution in steady jumps and what has been postulated for a non-constant form, periodic bore wave including the model used in this paper. The numerical model is discussed in Section 4. Section 5 gives the results of some laboratory measurements of inner surface zone waves used as input boundary conditions and to check the numerical experiments as discussed in Section 6.

2. Theory – Basic Equations

For non-permanent form propagating bores in a fixed reference frame, the four equation system employed by Svendsen and Madsen (1984) is (see Fig. 3) in conservation form:

conservation of mass,

$$\eta_t + Q_x = 0 \tag{2.1}$$

conservation of total momentum,

$$Q_t + \left(\int_{-h}^{\eta} u^2 dz + \tfrac{1}{2} g d^2 \right)_x = g d h_x \tag{2.2}$$

conservation of mean energy,

$$E_t + (E_f)_x = D \tag{2.3}$$

and the

momentum conservation in core region,

$$(u_0)_t + u_0 (u_0)_x + g \eta_x = 0 \tag{2.4}$$

where:

volumetric flowrate per unit width,

$$Q(x,t) \equiv \int_{-h}^{\eta} u \, dz \tag{2.5}$$

total water depth,

$$d(x,t) = h(x) + \eta(x,t) \tag{2.6}$$

energy density per unit surface area,

$$E(x,t) = \int_{-h}^{\eta} \tfrac{1}{2} u^2 dz + \tfrac{1}{2} g \eta^2 \tag{2.7}$$

flux of energy through a vertical slice,

$$E_f(x,t) = \int_{-h}^{\eta} \tfrac{1}{2} u^3 dz + g \eta Q \tag{2.8}$$

loss of mean energy to turbulence,

$$D(x,t) = \int_{-h}^{\eta} \overline{u'w'} \frac{\partial u}{\partial z} \, dz \tag{2.9}$$

with $u_0(x,t)$ the velocity in the lower constant-velocity, core region beneath the turbulent wedge with $\overline{u'w'}$ the Reynolds shear stresses resulting from the turbulence and correlated by ensemble averaging. The subscripts x or t means partial differentiation with respect to x or t.

The primary assumption is that the horizontal length scale of the motion is much larger than the vertical scale so that the vertical

momentum balance is omitted and consequently a hydrostatic pressure
distribution is taken. Normal turbulent stresses in (2.2) and bottom
generated turbulence and shear stress are also neglected.

    To solve the four equation system (2.1-2.4) requires relating the
turbulent shear stress, $\overline{u'w'}$ to the mean flow properties. The turbu-
lence closure methods employed permit local nonequilibrium between
turbulence advection and dissipation, but further details are beyond
the scope of this paper.

    This system (2.1-2.4) with closure represents one possible exten-
sion of the nonlinear shallow water equations (SWE) that includes the
effects of turbulence.

    Another approach as followed in this paper is to only invoke the
following two, depth-integrated conservation laws:

conservation of mass,

$$\eta_t + Q_x = 0 \qquad\qquad (2.10)$$

and

conservation of total momentum,

$$Q_t + \left(I + \tfrac{1}{2} g d^2\right)_x = g d h_x \qquad (2.11)$$

where:

momentum flux density,

$$I(x,t) \equiv \int_{-h}^{\eta} u^2 dz \qquad\qquad (2.12)$$

and the effects of turbulence are now singarilary brought in through
$I(x,t)$ which itself only depends on the mean velocity profile
$u(x,z,t)$. All the assumptions in the four equation system are retain-
ed. The problem reduces to finding $I(x,t)$.

    One possibility is to introduce a momentum flux correction coef-
ficient, $\alpha(x,t)$ so that

$$I(x,t) \equiv \frac{\alpha Q^2}{d} \qquad\qquad (2.13)$$

where

$$\alpha(x,t) \equiv \frac{d}{Q^2} \int_{-h}^{\eta} u^2 dz \qquad\qquad (2.14)$$

Now the problem is to find $\alpha(x,t)$ for non-permanent form, surf zone
waves. When $\alpha(x,t) = 1.0$, the SWE are recovered and the front face
continuously steepens with no turbulence effects since the velocity
profile remains uniform. In real propagating bores, water spills down
the front face generating turbulence at the toe and creating a strong-
ly non-uniform velocity profile, so that behind the toe $\alpha(x,t) > 1.0$.

3. Velocity and α-Distribution Models

It is instructive to review some typical $u(z)$ profiles and re-sulting α values as shown in Fig. 4. A log profile in uniform, open channel flow (Fig. 4b) gives $\alpha - 1.05$ (Chow, 1955). The roller of a hydraulic jump causes a flow reversal (Fig. 2 and Fig. 4c) and sig-nificantly enhances the total momentum flux. The extreme case is a complete flow reversal (Fig. 4d) which essentially doubles the momen-tum flux created by each half.

The velocity distribution $u(z)$ employed for this paper is the similarity profile used by Madsen and Svendsen (1983) for steady jumps:

$$f(\sigma) = \frac{u - u_o}{u_s - u_o} \qquad 0 \leqslant \sigma \leqslant 1 \qquad (3.1)$$

where

$$\sigma = \frac{z-d}{b} \qquad b = d-a \qquad (3.2)$$

with $u_s(x,t)$ at the free surface, and $b(x,t)$ the width of the turbu-lent wedge. The choice of $f(\sigma)$ depended somewhat on the turbulent closure and a third order polynomial of the form

$$f(\sigma) = -A\sigma^3 + (1+A)\sigma^2 \qquad (3.3)$$

with $A = 1.4$ was found to give a good fit to measured mean velocity profiles for a wide range of inlet Froude numbers, $F_1^2 = u_1^2/gd_1$, with u_1, d_1 the entrance jump conditions.

The α-distribution that results from the Madsen and Svendsen (1983) theory is found by putting (3.1-3.3) into (2.14) to give

$$\alpha_r(x) = \zeta\left[1 + \frac{1}{F_1^2}\left(1-\zeta^2\right)\right] \qquad \zeta = \frac{d(x)}{d_1} \qquad (3.4)$$

with $d(x)$ part of the solution for the jump profile. Here $\alpha_r(x)$ is the distribution for a steady hydraulic jump or a moving bore on a horizontal bottom in a relative coordinate system moving with the bore celerity (Fig. 2). Some typical distributions of $\alpha_r(x)$ for $F_1^2 = 3.0$, 3.95 and 8.0 are shown by the solid line in Fig. 6.

For a fixed coordinate system (Fig. 3) and the $\alpha(x)$ required by (2.11) and (2.13) it can be shown that

$$\alpha(x) = \left(\frac{h}{\eta}\right)^2\left(\alpha_r - 1\right) + 1 \qquad (3.5)$$

For example, when $F_1^2 = 3$ (a weak jump) and at $\eta/h = 0.3$, then $\alpha_r = 1.2$ and $\alpha = 3.2$. The turbulence significantly alters the velocity profile and enhances the momentumn flux.

For constant form steady jumps and propagating bores, the water depth gradually increases so that α_r gradually rises above 1.0 to a peak value α_p within the jump at some distance x_p from the toe then gradually decreases back to 1.0 downstream. This is shown

(a) u = CONSTANT   (b) u(z) = LOGARITHMIC (c) u(z) REVERSES (d) FULL REVERSAL

$\alpha \cong 1.0$ $\alpha \approx 1.05$ $\alpha > 1.0$ $\alpha \gg 1.0$
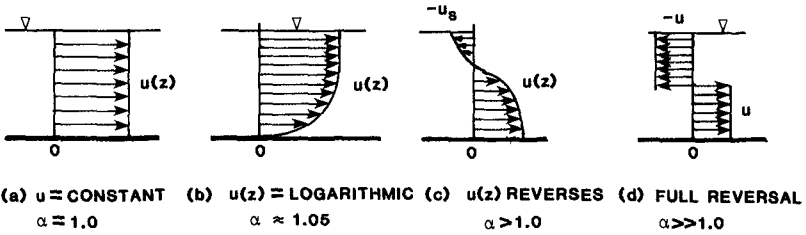
Fig. 4 Some velocity profiles and resulting momentum coefficients.
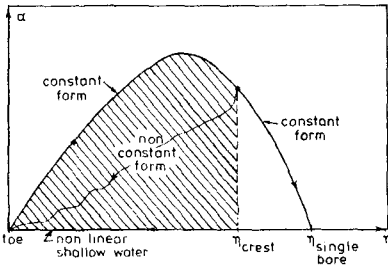
Fig. 5 Schematic variation of momentum coefficient α with downstream
water surface elevation η. (after Madsen, 1981)
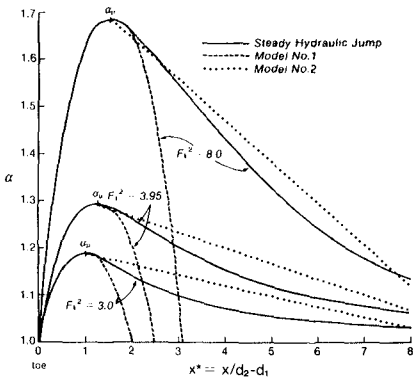
Fig. 6 Typical momentum coefficient distributions. The solid line is
for the hydraulic jump. The dashed line (Model No. 1) is for
a propagating wave-like bore of nonuniform shape. Model No.
2 is a variation not tested.

schematically in Fig. 5 (from Madsen, 1981) and for typical values in
Fig. 6. The theory was exercised for a large range of F_1^2 values and
least squares curve fitting employed to find that for constant form
jumps

$$\alpha_p(F_1^2) = 0.098\,F_1^2 + 0.902$$

and

$$X_p(F_1^2) = \begin{cases} 0.3\,F_1^2 + 0.05 & F_1^2 \leqslant 4 \qquad (3.6) \\ 0.0833\,F_1^2 + 0.92 & F_1^2 > 4 \qquad (3.7) \end{cases}$$

But what is the $\alpha_r(x)$ distribution beneath non-permanent form,
surf zone waves? Experimental evidence (Svendsen, et al., 1978) sug-
gests that surf zone waves have similar-shaped fronts but changing
backs as the broken wave shoals and dissipates energy up a slope.
Fig. 5 schematically illustrates that non-constant form waves have an
$\alpha_r(x)$ distribution that must return to 1.0 as $\eta(x)$ also decreases.
This suggests an α_r-distribution similar to the steady, constant form
jumps up to α_p on the front side (from trough to near the crest) but
then rapidly decreasing again on the back side.

The initial, empirical α_r-distribution chosen for this study was
a parabolic shape as shown by the dashed line in Fig. 6 and labeled
Model No. 1. The vertex (α_p, x_p) was found from (3.6) and (3.7) as key
variables in the parabolic distribution with one limb passing through
the toe ($x=0$, $\alpha=1.0$). A procedure to theoretically calculate the
$I(x,t)$ distribution can be developed from the four equation system of
Svendsen and Madsen (1984). Model No. 2 (Fig. 6, dotted) was never
tested.

4. Numerical Model

An explicit, finite-difference code based on the Lax-Wendroff,
2-Step algroithm (LW2S) has been developed for numerical solution of
(2.10) and (2.11) using (2.13) and the parabolic model for the $\alpha(x)$
distribution. The code uses the method of characteristics and inter-
polation subroutines to provide the needed additional boundary data.
For example, when $\eta(t)$ is specified on the incoming boundary, the code
calculates $Q(t)$ values at upper level time steps on the boundary as
required by the LW2S algorithm. At the opposite, outgoing boundary a
radiation boundary condition together with excessive numerical dissi-
pation is introduced over a short reach to prevent wave energy reflec-
tions.

A large number of initial and boundary conditions with $\alpha(x,t) =$
1.0 giving known analytical solutions for simple cases were employed
during development and testing to insure the validity of the code and
given confidence in the results.

The toe location was a key variable in the model since the para-
bolic α-distribution began from this point. For a steady jump or con-
stant form bore the toe is well defined since fixed in space. For the
non-permanent form bore on a sloping bed, Svendsen and Madsen (1984)
used as initial conditions a permanent bore starting seaward of the

slope with well defined toe. They then propagated the toe point it-
self at a celerity calculated by

$$C = \frac{Qx}{\eta_x} \approx \frac{Q_j - Q_{j-1}}{\eta_j - \eta_{j-1}} \tag{4.1}$$

as a first order, upwind difference with j as the first grid point be-
hind the toe.

For surf zone waves the toe position is ill defined since the ap-
proaching trough is a continuously varying curve. The toe position
for these initial tests was heuristically taken midway between the
trough (maximum negative η) and the maximum front face slope. This
was from observations in the laboratory that showed the toe point
slightly up the curved trough. The toe position was then reesta-
blished by this procedure each time step rather than propagating the
initial toe position. This method proved to be expensive on the com-
puter and caused problems as discussed in Section 7.

To numerically calculate F_1^2 and hence α_p and x_p to derive the
α-distribution, (4.1) was employed to calculate C, but with j at the
point of maximum slope. The relative volumetric flowrate, Q_m was
found from

$$Q_m = cd - Q \tag{4.2}$$

and finally

$$F_1^2 = \frac{Q_m^2}{gd^3} \tag{4.3}$$

with d and Q taken at the trough position to give an overall, repre-
sentative value of F_1^2.

5. ISVA Experiments

Results of laboratory experiments at the Institute of Hydrodyna-
mics and Hydraulic Engineering (ISVA), Denmark as performed by Hansen
(1980,1982) were adapted for numerical testing. The experiments were
made in a 60 cm wide, 32 m long and 36 cm deep (SWL) wave basin with a
1:34 plane sloping beach. Twelve wave gages spaced throughout the in-
ner surf zone monitored the change in wave height and shape. Of the
twenty test runs available, one test with wave period, T = 2.22 sec
and initial, "deepwater" wave height, $H_0 = 10$ cm was selected for
numerical simulation. Within the surf zone, surface wave measurements
averaged over 20 waves at the first gage (CHANNEL 00, Hi = 5.48 cm)
became the boundary data as input into the numerical model.

The experimentally measured results of this particular test (Run
No. 201) are summarized in Fig. 7 for relative variation of wave
height, H/Hi versus distance up the slope and in Fig. 8 for the wave
shape at four selected locations. The last gage (CHANNEL 11) was
located 2.8 m from the first gage (CHANNEL 00). Fig. 8 shows rapidly
changing back side slopes of these waves whereas the front slopes are
relatively unchanged. The wave is clearly of non-constant form.
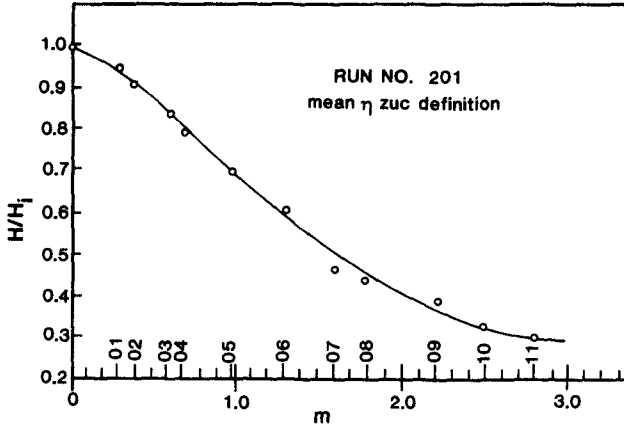
Fig. 7   Relative wave height versus position up the beach for run no.
         201. (courtesy J.B. Hansen, 1982)
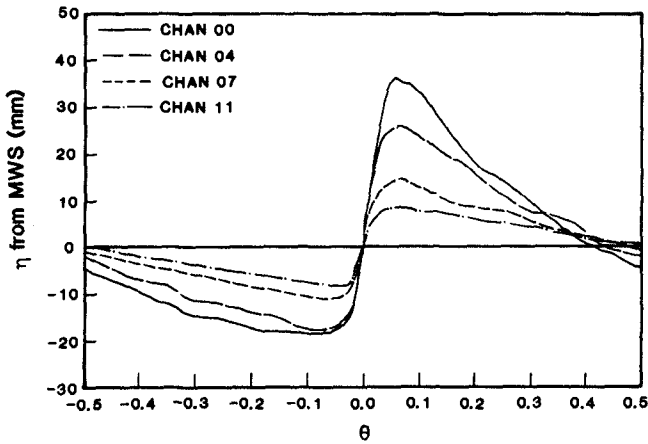
Fig. 8   Variation of wave shape at four locations for run no. 201.
         (courtesy J.B. Hansen, 1982)

Further details regarding the facilities, instrumentation and data anlaysis procedures employed can be found in Hansen and Svendsen (1979).

6. Numerical Experiments

The numerical experiments investigated the initial shape and wave height changes and celerity of the broken wave (labelled CHAN 00 in Fig. 8) as it shoaled and dissipated energy further up the beach. The detailed wave profile used as input boundary conditions is shown in Fig. 9. An arbitrary, smaller wave was placed in the "numerical" wave basin as initial conditions to avoid a completely "cold start" condition. Mean water depth (MWS) from the laboratory experiments which included wave induced setup was used as datum.

For an incoming wave length of about 2.5 m, the use of $\Delta x = 0.025$ m gave roughly 50 grid intervals per wave for the staggered computational mesh of the LW2S scheme. This resulted in very low numerical dissipation. The $\Delta t = 0.014$ sec was determined by using the maximum expected wave celerity together with the Courant number, $Cr<1.0$ restriction inherent in all explicit numerical schemes. As a result, for a wave perod, $T = 2.22$ sec, $N = 80$ time steps correspond to about one-half a wave cycle. The shoreline ($d = 0$) is about 3.3 m from the input boundary or at a grid index $j = 133$.

Fig. 10 is a baseline test result. It shows a wave propagating from left to right up the beach for the case when $\alpha(x,t) = 1.0$ for all time and space and represents a solution to the SWE. The wave shoals and a secondary wave forms behind as the front face steepens. No mechanism exists in the numerical model to dissipate energy. The reason for the formation of the secondary wave is unclear but may be due to the original input wave shape (Fig. 9); the nonlinear advection term in the SWE creating harmonic components or, there being no real mechanism in the model to dissipate higher wave number energy. Running longer caused the scheme to go unstable. Fig. 11 demonstrates the use of a numerical smoothing filter on these results where

$$\eta_j^n = \gamma \, \eta_{j+1}^n + (1-2\gamma)\eta_j^n + \gamma \eta_{j-1}^n \qquad (6.1)$$

with $\gamma = 0.125$, and using the filter every other time step (NR=2) or every ten time steps (NR=10). The use of this filter smoothed out the smaller oscillations and permitted the scheme to run beyond a full wave cycle. The crest elevation at N=80 is 0.063 m and 0.046 after filtering. This filter behaves as an energy dissipative mechanism to remove higher wave energy (like turbulence) and changes the front face slope but not the phase speed of the wave.

Figures 12 and 13 show analogous plots but now with Model No. 1 used for the parabolic α-distribution beneath the wave crest so that $\alpha(x,t)$ varies in space and time. The effect of broken wave generated turbulence alters the velocity profile to enhance the momentum flux beneath the wave crest and behind the toe of the bore. Fig. 12 includes the numerical filter (NR=10) to give a smoothed, clearer picture of the wave shape changes. The wave is seen to initially shoal
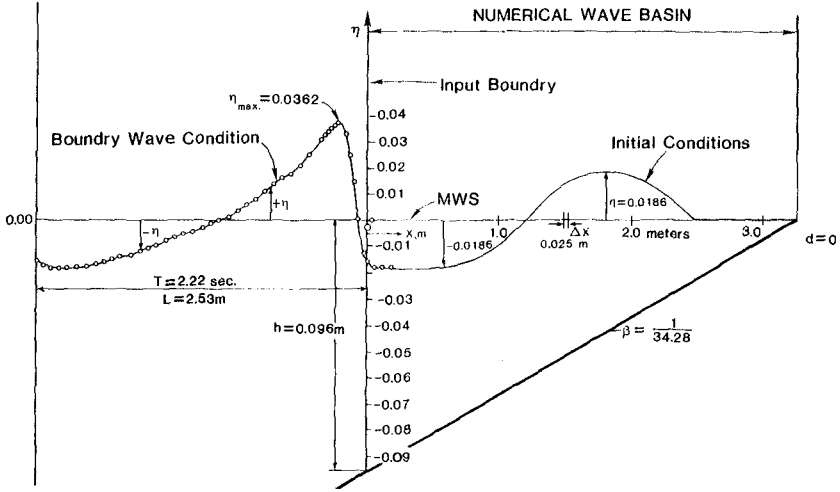
Fig. 9   Initial conditions and input wave boundary conditions for
         numerical simulation.
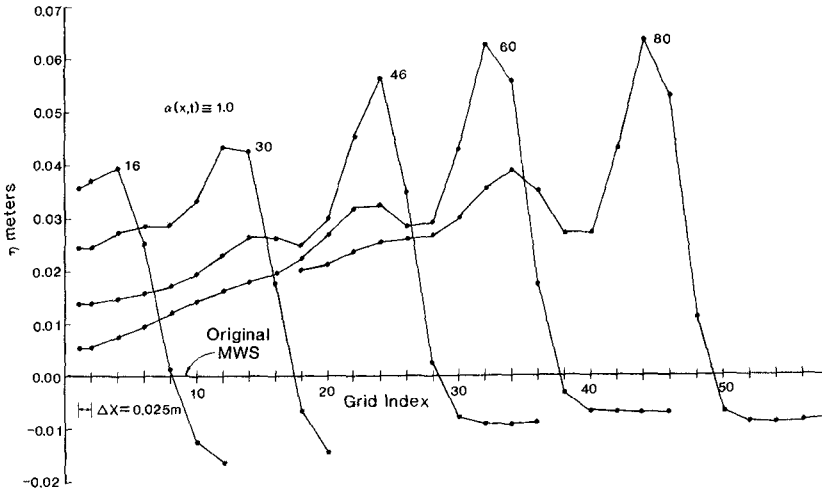
Fig. 10 Basline numerical test results with no turbulence (α=1.0) for
         the five time steps. N=80 equivalent to one-half wave
         period. A 2.22 sec wave with initial height of 0.055 m moves
         up a 1:34 slope.
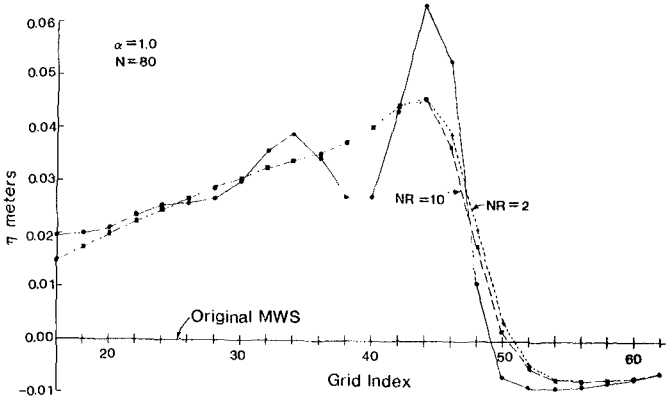
Fig. 11   Same as Fig. 10 at N=80 except includes use of numerical
          filter every other (NR=2) and every ten (NR=10) time steps.
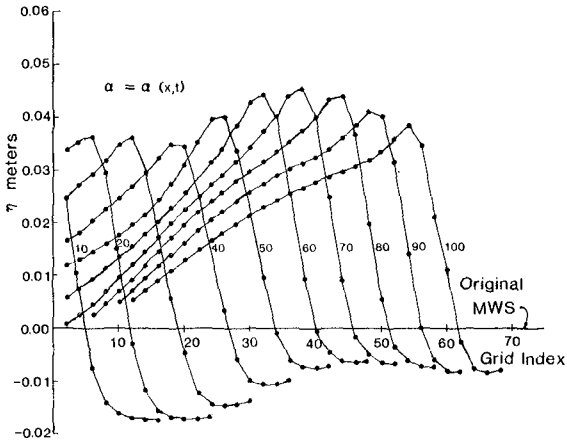
Fig. 12   Numerical test results with parabolic α-distribution (Model
          No. 1) for 10 different time steps.
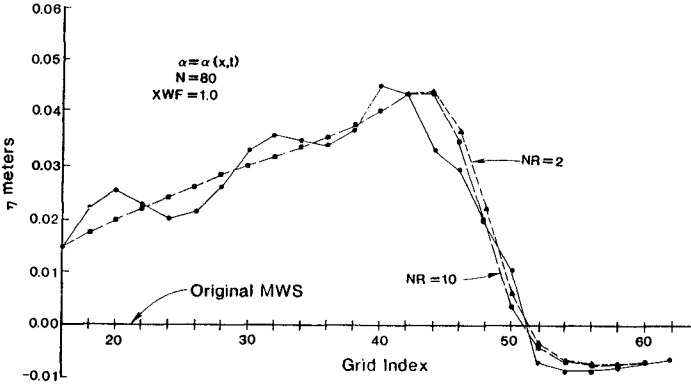
Fig. 13   Same as Fig. 12 at N=80 including raw results and the effect
          of numerical filters.
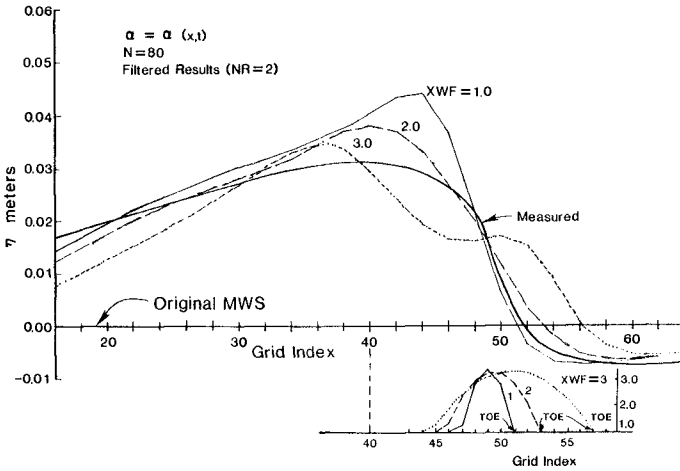
Fig. 14   The effect of different widths of the parabolic, α–
          distribution model on the wave shape at N=80. Double width
          (XWF=2) and trebled width (XWF=3) shapes are shown below.
          Also shown is the laboratory measured wave shape as thick
          solid line.

in crest elevation (while dissipation takes place) and the trough elevation also rises. This is felt to be due to the initial conditions in the numerical basin. Beyond N=70, the numerical wave has established some type of equilibrium within the basin and dissipation dominates. Fig. 13 shows the wave shape after N=80 time steps (one-half period) and demonstrates that high wave number oscillations (solid line) are still present when no numerical filtering is employed. Clearly, Fig. 13 reveals that the α-distribution model must be responsible for the wave crest elevation reduction for now η_{max} = 0.045 m as compared to η_{max} = 0.063 m for the SWE (α =1.0) and the unfiltered results. It is also evident in Fig. 13 that additional numerical smoothing actually increases the front face steepness while smoothing out the higher wave number oscillations. Thus although both the α-distribution mechanism and the numerical smoothing effectively result in energy dissipation, the general wave shape changes are primarily controlled by the $\alpha(x,t)$ model.

This is demonstrated further in Fig. 14 for three different widths of the α-distribution model. The results again show the wave shape at N=80 with numerical filtering included. The width of the parabolic α-distribution is arbitrarily doubled (XWF=2) and trebled (XWF=3) and this results in a significant change in both the crest elevation and slope of the front face. The α-distributions are also shown below the wave with the toe located as discused in Section 4. Widening the α- distribution is seen to flatten the front shape. Entirely different results would be expected if the initial toe position were itself propagated as part of the solution procedure.

The thick solid line in Fig. 14 is from the measured laboratory results at a comparable position in space. The wave profile in time was converted to a space profile using the celerity of a local measured bore wave as reference. This wave was taken from the CHANNEL 05 position (see Fig. 7) so that the comparison is not exact. The measured shape in Fig. 14 is only included to give some rough idea of how the numerically calculated wave compares with that reported from the laboratory measurements.

7. Summary

This paper summarizes initial efforts to model surf zone wave shoaling and energy dissipation through the use of a semi-empirical, momentum correction coefficient distribution, $\alpha(x,t)$ in the nonlinear SWE. The qualitative trends are correct in that energy is lost and the wave shape stabilizes rather than steepening. The numerical model can be improved by independently propagating the initial toe position as part of the solution procedure and by the development of a more rational theory for the $\alpha(x)$-distribution beneath the wave. In addition, many more waves need to be propagated through the numerical basin to reach an equilibrium state as found in the laboratory basin in order to make a proper comparison. Some additional energy loss occurs in boundary layer shear that should also be accounted for in the numerical model.

Further research is needed to theoretically determine the appropriate $\alpha(x,t)$-distribution.

References

Chow, V.T. (1955) Open Channel Hydraulics, McGraw-Hill, NY.

Hansen, J.B. (1980) "Experimental Investigations of Periodic Waves Near Breaking", Proceedings, 17th Int'l Conf. Coastal Engng., Sydney.

Hansen, J.B. (1982) Personal communication.

Hansen, J.B. and I.A. Svendsen (1979) "Regular Waves in Shoaling Water - Experimental Data", Series Paper 21, ISVA, Technical Univ. Denmark, Lyngby.

Hibberd, S. and D.H. Peregrine (1979) "Surf and Run-Up on a Beach: A Uniform Bore", J. Fluid Mech., Vol. 95, No. 2, pp. 323-345.

Lax, P.D. and Wendroff (1960) " Systems of Conservation Laws", Comm. Pure and Applied Math., Vol. 13, pp. 217-237.

Madsen, P.A. (1981) "A Model for a Turbulent Bore", Series Paper 28, ISVA, Technical Univ. Denmark, Lyngby.

Madsen, P.A. and I.A. Svendsen (1983) "Turbulent Bores and Hydraulic Jumps", J. Fluid Mech., Vol. 129, pp. 1-25.

Meyer, R.E. and A.D. Taylor (1972) "Run-Up On Beaches" in Waves on Beaches and Resulting Sediment Transport, Academic Press, NY, pp. 357-411.

Peregrine, D.H. and I.A. Svendsen (1978) 'Spilling Breakers, Bores and Hydraulic Jumps", Proceedings, 16th Int'l. Conf. Coastal Engng., Vol. I, pp. 540-550.

Svendsen, I.A., P.A. Madsen and J.B. Hansen (1978) "Wave Characteristics in the Surf Zone", Proceedings, 16th Int'l. Conf. Coastal Engng., Vol. I, pp. 520-539.

Svendsen, I.A. and P.A. Madsen (1984) "A Turbulent Bore on a Beach", J. Fluid Mech., in review.